applied sciences

MDPI

Article

Prediction of Ultimate Bearing Capacity of Shallow Foundations on Cohesionless Soils: A Gaussian Process Regression Approach

Mahmood Ahmad [1,2,†], Feezan Ahmad [3,†], Piotr Wróblewski [4,5], Ramez A. Al-Mansob [1,*], Piotr Olczak [6], Paweł Kamiński [7], Muhammad Safdar [8] and Partab Rai [9]

1 Department of Civil Engineering, Faculty of Engineering, International Islamic University Malaysia, Jalan Gombak, Selangor 50728, Malaysia; ahmadm@iium.edu.my
2 Department of Civil Engineering, University of Engineering and Technology Peshawar (Bannu Campus), Bannu 28100, Pakistan
3 State Key Laboratory of Coastal and Offshore Engineering, Dalian University of Technology, Dalian 116024, China; ahmadf@mail.dlut.edu.cn
4 Faculty of Engineering, University of Technology and Economics H. Chodkowska in Warsaw, Jutrzenki 135, 02-231 Warsaw, Poland; piotr.wroblewski@wat.edu.pl or piotr.wroblewski@uth.edu.pl
5 Faculty of Mechatronics, Armament and Aerospace of the Military University of Technology, Sylwestra Ka-liskiego 2, 00-908 Warsaw, Poland
6 Mineral and Energy Economy Research Institute, Polish Academy of Sciences, Wybickiego St. 7A, 31-261 Kraków, Poland; olczak@min-pan.krakow.pl
7 Faculty of Mining and Geoengineering, AGH University of Science and Technology, 30-059 Kraków, Poland; pkamin@agh.edu.pl
8 Earthquake Engineering Center, University of Engineering and Technology Peshawar, Peshawar 25000, Pakistan; drsafdar@uetpeshawar.edu.pk
9 Key Laboratory of Transportation Tunnel Engineering, Ministry of Education, School of Civil Engineering, Southwest Jiaotong University, Chengdu 610031, China; partabrai@my.swjtu.edu.cn
* Correspondence: ramez@iium.edu.my
† These authors contributed equally to this work.

Abstract: This study examines the potential of the soft computing technique—namely, Gaussian process regression (GPR), to predict the ultimate bearing capacity (UBC) of cohesionless soils beneath shallow foundations. The inputs of the model are width of footing (B), depth of footing (D), footing geometry (L/B), unit weight of sand (γ), and internal friction angle (ϕ). The results of the present model were compared with those obtained by two theoretical approaches reported in the literature. The statistical evaluation of results shows that the presently applied paradigm is better than the theoretical approaches and is competing well for the prediction of UBC (q_u). This study shows that the developed GPR is a robust model for the q_u prediction of shallow foundations on cohesionless soil. Sensitivity analysis was also carried out to determine the effect of each input parameter.

Keywords: cohesionless soil; machine learning; Gaussian process regression; shallow foundation; ultimate bearing capacity

check for updates

Citation: Ahmad, M.; Ahmad, F.; Wróblewski, P.; Al-Mansob, R.A.; Olczak, P.; Kamiński, P.; Safdar, M.; Rai, P. Prediction of Ultimate Bearing Capacity of Shallow Foundations on Cohesionless Soils: A Gaussian Process Regression Approach. *Appl. Sci.* **2021**, *11*, 10317. https://doi.org/10.3390/app112110317

Academic Editors: Guoliang Dai, Fayun Liang and Xinjun Zou

Received: 24 September 2021
Accepted: 1 November 2021
Published: 3 November 2021

1. Introduction

Ultimate bearing capacity (UBC) and allowable settlement are two important criteria to consider when designing shallow foundations. The UBC is governed by the shear strength of the soil and is estimated by theories proposed by Terzaghi [1], Meyerhof [2], Hansen [3], Vesic [4], etc. However, the various bearing capacity equations reveal a wide range of variations. Furthermore, the proposed bearing capacity theories include a number of assumptions that contribute to simplifying the problems [5].

Numerous studies proposed numerical approaches for estimating bearing capacity in addition to semi-empirical solutions for determining the bearing capacity of foundations,

e.g., [6,7]. Models are usually validated using the model-scale footing test. A number of researchers have investigated that how to reduce scale effects when extrapolating experimental results to full-scale footings (e.g., de Beer [8]; Yamaguchi et al. [9]). In model-scale footing experiments, Tatsuoka et al. [10] studied how particle size affects the UBC. The shearing strains vary significantly along the slip line, according to the results of large-scale footing tests on dense sand. As a result, bearing capacity formulas that use the maximum value of friction angle, (ϕ_{max}) tend to overstate prototype bearing capacities [11]. Therefore, the actual model-scale footing test findings differed from theoretical equations, and special consideration should be given when comparing model-scale footing test results with full-scale foundation behavior. For this reason, a new approach is needed to ensure more accurate predictions of actual bearing capacity.

Intelligent systems are typically used to model complex interactions between inputs and outputs or to explore patterns in available data. Artificial intelligence (AI)-based methods are capable of capturing the problem's inherent nonlinearity and complex interaction between the involved variables in various domains, e.g., [12–21]. These approaches can be trained to learn the relationship between soil mechanical properties and foundation geometry with foundation bearing capacity, and no prior knowledge of the relationship's form. Different forms of AI-based techniques have recently been used by different researchers to address the UBC problem of shallow foundations. Artificial neural networks (ANNs), fuzzy inference systems (FISs), adaptive neuro-fuzzy inference systems (ANFISs), ant colony optimization (ACO), genetic programming (GP), weighted genetic programming (WGP), soft-computing polynomials (SCP), support vector machine (SVM), random forest (RF), and relevance vector machine (RVM) have all been used to successfully estimate the UBC of shallow foundations on soil [11,22–26]. Soft computing methodologies are more accurate than analytical formulas, according to all of these studies. The findings revealed that the ML models mentioned above are capable of obtaining the experimental observations with acceptable accuracy. However, this field continues to be further explored.

The Gaussian process regression (GPR) approach has been successfully applied in many domains, e.g., [27–29], but its application in geotechnical engineering is limited based on literature surveys. Considering the improved performance of GPR, it is, however, used for the first time in this study to predict the UBC of shallow foundations on cohesionless soils. To demonstrate the efficacy of the proposed GPR-based model, the results were compared with various well-known classical formulas for calculating the UBC.

The main contributions of this paper are as follows:

- To examine the capability of the GPR model for the prediction of q_u of shallow foundation on cohesionless soil;
- To undertake a comparative study with the commonly used bearing capacity theories;
- To conduct sensitivity analyses for the determination of the effect of each input parameter on q_u.

The structure of the paper is as follows: In Section 2, the theoretical background of ultimate bearing capacity is presented. The numerical model and verification are described in Section 3. Section 4 presents the construction process of the prediction model. In Section 5, results and discussion are described. Finally, the concluding remarks are presented.

2. Theoretical Background of Ultimate Bearing Capacity

Prandtl [30] and Reissner [31] developed plastic theory-based methods for determining the ultimate bearing capacity of shallow strip footings. Over the years, other researchers significantly improved the formulation [1,2,4,22,32,33]. Terzaghi [1] improved Prandtl's theory [30] by using the principle of superposition to account for the soil weight. Taylor [32] incorporated the effect of the overburdened soil surcharge at the foundation level into Prandtl's formulation. Meyerhof [2] extended Terzaghi's bearing capacity equation by incorporating different shape and depth factors. Hansen [3] later updated the Meyerhof model. Vesic [4] provided a bearing capacity prediction equation that was similar to Hansen's equation. Table 1 summarizes the general forms of the classical equations. The

form of the equations presented by the other researchers remained the same as Terzaghi's, as can be seen in this table. Meyerhof [2], Hansen [3], Vesic [4], and other researchers proposed different shape, depth, inclination, ground, and base factors for the bearing capacity equations after thorough in situ and laboratory tests. However, one of the primary shortcomings of these traditional formulations is that they are based on some simplifying assumptions. As a result, they do not always produce accurate bearing capacity estimates [22,34].

Table 1. General forms of the classical prediction equations for the bearing capacity of shallow foundations.

Reference	Equation
Terzaghi [1]	$q_u = cN_c s_c + \gamma D N_q + \frac{1}{2}\gamma B N_\gamma s_\gamma$ $N_c = (N_q - 1)\cot\phi$ $N_q = \frac{a^2}{a\cos^2(45+\phi/2)}$ $a = e^{(0.75\pi-\phi/2)\tan\phi}$ $N_\gamma = \frac{\tan\phi}{2}\left(\frac{K_{p\gamma}}{\cos^2\phi} - 1\right)$
Meyerhof [2]	$q_u = cN_c s_c d_c + \gamma D N_q s_q d_q + \frac{1}{2}\gamma B N_\gamma s_\gamma d_\gamma$ $N_q = e^{\pi\tan\phi}\tan^2\left(45 + \frac{\phi}{2}\right)$ $N_\gamma = (N_q - 1)\tan(1.4\phi)$ $N_c = (N_q - 1)\cot\phi$
Hansen [3]	$q_u = cN_c s_c d_c i_c g_c b_c + \gamma D N_q s_q d_q i_q g_q b_q + \frac{1}{2}\gamma B N_\gamma s_\gamma d_\gamma i_\gamma g_\gamma b_\gamma$ N_q = same as Meyerhof above N_c = same as Meyerhof above $N_\gamma = 1.5(N_q - 1)\tan\phi$
Vesic [4]	Same as Hansen's equation N_q = same as Meyerhof above N_c = same as Meyerhof above $N_\gamma = 2(N_q + 1)\tan\phi$

Notes: q_u: ultimate bearing capacity of footing; c: cohesion; γ: average effective unit weight of the soil below and around the foundation; B: width of footing; D: depth of footing; N_c, N_q, and N_γ: non-dimensional bearing capacity factors as exponential functions of ϕ; ϕ: internal friction angle; s_c, s_q, and s_γ: non-dimensional shape factors; i_c, i_d, and i_γ: non-dimensional inclination factors; d_c, d_q, and d_γ: non-dimensional depth factors; g_c, g_q, and g_γ: non-dimensional ground factors (base on slope); b_c, b_q, and b_γ: base factors (tilted base).

3. Materials and Methods

3.1. Dataset

The data used in this study were adopted from Padmini et al. [11]. The five input parameters used for model development in this study were width of footing (B), depth of footing (D), footing geometry (L/B), unit weight of sand (γ), and internal friction angle (ϕ). Ultimate bearing capacity (q_u) was the single output. The data thus compiled comprised a total of 97 datasets, which consisted of results of load test data of square, rectangular, and strip footings of different sizes tested in sand beds of various densities.

The data were divided into training and testing sets, which is a method that has a substantial impact on the results when using data mining techniques [35,36]. In this case, the entire database was divided into multiple random combinations of training and testing sets until both training and testing sets had a robust representation of the entire population. A statistical analysis of the input and output parameters of the randomly selected training and testing sets was carried out to identify the most robust representation. The purpose of this analysis was to assure that the statistical properties of the data in each of the subsets were as close as possible, indicating that they represented the same statistical population. This was achieved using a trial-and-error method in this work. For the construction and testing of the GPR model, the best statistically consistent combination was selected. The data division was performed in such a way that 78 (80%) were used for training, and 19 (20%) were used for testing in all the experiments considered in this study. The parameters used in the statistical analysis included maximum, minimum, mean, and

standard deviation. The results of the statistical analysis of the finally selected combinations are shown in Table 2. It should be mentioned that due to the fact that the data contained singular, rare events that could not be replicated in all cases of the dataset, there may still have been some minor inconsistencies in the statistical parameters for the training and validation sets. The descriptive statistics (such as minimum and maximum values, mean, and standard deviations) of the selected UBC parameters with the established GPR model are provided in Table 2 (the complete database is available in Table A1).

Table 2. Statistical aspects of the dataset.

Dataset	Statistical Parameter	B (m)	D (m)	L/B	γ (kN/m^3)	ϕ (°)	q_u (kPa)
Training	Minimum	0.0585	0	1	9.85	32	58.5
	Maximum	3.016	0.889	6	17.1	44.8	2847
	Mean	0.398	0.156	3.126	14.279	38.492	407.899
	Standard deviation	0.543	0.195	2.192	2.642	3.308	511.870
Testing	Minimum	0.0585	0	1	10.2	32	91.5
	Maximum	1.492	0.762	6	17.1	44.8	2033
	Mean	0.420	0.204	2.995	13.777	38.800	569.826
	Standard deviation	0.361	0.221	1.964	2.573	3.225	600.020

3.2. Correlation Analysis

The strength of the correlation between the various factors was verified using correlation coefficients (ρ) (see Table 3). The following formula for ρ is given a pair of random variables (x,y):

$$\rho(x,y) = \frac{\mathrm{cov}(x,y)}{\sigma_x \sigma_y} \quad (1)$$

where cov is the covariance, σ_x is the standard deviation of x, and σ_y is the standard deviation of y. $|\rho| > 0.8$ indicates a strong correlation between x and y, values between 0.3 and 0.8 indicates a moderate connection, and $|\rho| < 0.30$ indicates a weak correlation [37]. A correlation is regarded as "strong" if $|\rho| > 0.8$, according to Song et al. [38]. Table 3 shows the correlations between B, D, L/B, γ, ϕ, and q_u, in order of moderate to weakest. As a result, no factors were removed from the UBC of the cohesionless soil estimation model. Table 3 shows that the maximum absolute value of the correlation coefficient is 0.710, and there is no "strong" correlation between the various pairs of factors.

Table 3. Correlation coefficients between various factors.

Parameter	B	D	L/B	γ	ϕ	q_u
B	1.000					
D	0.710	1.000				
L/B	−0.351	−0.249	1.000			
γ	−0.269	−0.125	0.340	1.000		
ϕ	−0.378	−0.286	0.124	0.076	1.000	
q_u	0.452	0.671	−0.248	−0.238	0.258	1.000

3.3. Gaussian Processes Regression

Gaussian processes regression (GPR) is a suitable and recently proposed method that has been used in a variety of machine learning applications [39]. The GPR model's probabilistic solution leads to the identification of generic regression problems using kernels. The applied regressor's training process can be categorized as Bayesian framing, and the model relations are presumed to follow a Gaussian distribution to encode the previous information about the output function [40]. The Gaussian process is defined

by a set of variables for which each one has a joint Gaussian allocation [41]. The overall structure of the Gaussian process is described by the following equation:

$$g(x) \sim GP\left(w(x), k\left(x, x'\right)\right) \tag{2}$$

The mean function of the Gaussian process is denoted by $w(x)$, and the kernel function is denoted by $k(x, x')$. The mean function is typically constant, either zero or the mean of the training dataset. In this study, the mean of the training dataset was used. Consider a learning dataset with N pairs in the form of $S = \{(x_i, y_i) \mid i = 1, 2, \ldots, N\}$ where x is an N-dimensional input vector, and y is the corresponding target. Using x_j as a test sample, the GPR model utilizes the below formulation in determining the relationship between the provided inputs and targets [41].

$$w_j = k_j^T \left[K(X, X) + \sigma^2{}_n I\right] y \tag{3}$$

$$\sigma_j^2 = k\left(x_j, x_j\right) - k_j^T \left[K(X, X) + \sigma_n^2 I\right]^{-1} k_j \tag{4}$$

where w_j denotes the mean value of the most compatible predicted outputs for the test input vector (x_j). Additionally, $K(X, X)$, k_j, σ_n^2 and y represent covariance matrix, the kernel distance between training and testing data, the noise variance, and the training observation, respectively. Furthermore, the produced variance $\left(\sigma_j^2\right)$ by Equation (4) indicates a confidence measure for the acquired results. It is worth noting that this variance is inversely proportional to the confidence associated with the w_j [42]. The formulas above can be combined in the form of a linear combination of the kernel function and the mean estimation $\overline{f}\left(x_j\right)$ as follows:

$$\overline{f}\left(x_j\right) = \sum_{i=1}^{s} \left(K(X, X) + \sigma^2{}_n I\right)^{-1} y k\left(x_j, x_j\right) \tag{5}$$

GPR utilizes a number of kernel functions. GPR has a limitation in terms of selecting a suitable kernel function. Pearson VII kernel function (*PUK*), a widely utilized kernel function, was chosen for GPR model construction in this study, as it has shown optimized results in predicting river discharge [43].

$$PUK = \left(1 / \left[1 + \left(2\sqrt{\|x_i - x_j\|}^2 \sqrt{2^{(1/\omega)} - 1} / \sigma\right)^2\right]^{\omega}\right) \tag{6}$$

where ω and σ are kernel parameters.

3.4. Model Evaluation and Comparison

To validate and compare the developed model, four quantitative statistics were used to assess the performance of the evaluation methods: coefficient of determination (R^2), the ratio of the root-mean-square error (*RSR*) to the standard deviation of measured data, Nash–Sutcliffe coefficient (*NSE*), and mean bias error (*MBE*). The following equations are used to express these indices:

$$R^2 = 1 - \frac{\sum_{i=1}^{n} \left(y_i - \hat{y}_i\right)^2}{\sum_{i=1}^{n} \left(y_i - \hat{y}\right)^2} \tag{7}$$

$$RSR = \frac{\sqrt{\sum_{i=1}^{n}(y_i - \hat{y}_i)^2}}{\sqrt{\sum_{i=1}^{n}(y_i - \overline{y})^2}} \quad (8)$$

$$NSE = 1 - \frac{\sum_{i=1}^{n}(y_i - \hat{y}_i)^2}{\sum_{i=1}^{n}(y_i - \overline{y})^2} \quad (9)$$

$$MBE = \frac{1}{n}\sum_{i=1}^{n}(\hat{y}_i - y_i) \quad (10)$$

In the equations, n is the number of data, y_i and $\hat{y}_i$ are the actual and predicted output of ith sample of the data, respectively; $\overline{y}$ is the averaged actual output of the data. The R^2 coefficient goes from 0 to 1, with a higher R^2 value indicating a more efficient model. When R^2 is larger than 0.8 and nearer to 1, the model is considered effective [44]. The *NSE* scale runs from $-\infty$ to 1, with 1 being a perfect match. An *NSE* value of more than 0.65 indicates a strong correlation [45,46]. The root-mean-square error (*RMSE*) observations' standard deviation ratio is calculated as the ratio of the *RMSE* and standard deviation of measured data. The *RSR* varies from an optimal value of 0 to a significant positive value. A lower *RSR* signifies a lower *RMSE*, indicating the higher predictive efficiency of the model. *RSR* classification ranges were described as very good, good, acceptable and unacceptable with ranges of $0.00 \leq RSR \leq 0.50$, $0.50 \leq RSR \leq 0.60$, $0.60 \leq RSR \leq 0.70$ and $RSR > 0.70$, respectively [47]. It is self-evident that the lower the *RSR* criteria is, the better is the model.

4. Construction of Prediction Model

The construction process of the prediction model is shown in Figure 1. First, 80% and 20% of the UBC data were selected based on statistical consistency as training and test sets, respectively. Second, using the optimal hyperparameters configuration, the prediction model was fitted based on the training set using the trial-and-error method. We adjusted the hyperparameters so as to maximize the likelihood of the training data. We initialized the hyperparameters to random values (in a reasonable range) and then used an iterative method to search for optimal values of the hyperparameters. Numerous trials were carried out to find optimal values of primary kernel parameters—omega (ω) and sigma (σ)—and the values were 1 in the GPR model. Fourth, the test set was adopted to judge the performance of the proposed GPR model according to the four standard statistical measures: R^2, *RSR*, *NSE*, and *MBE*. Higher values of R^2 and *NSE*, and lesser values of *RSR*, indicate a better estimation accuracy of the proposed model. Last, the developed model was compared with the commonly used bearing capacity theories by comparing the comprehensive performance if the prediction performance of this model was acceptable, then it could be adopted for deployment and made sensitivity analysis. The entire calculation process was performed in Waikato Environment for Knowledge Analysis (WEKA) software [48]. In this study, for the GPR model, the Pearson VII function-based universal kernel [49] was used.

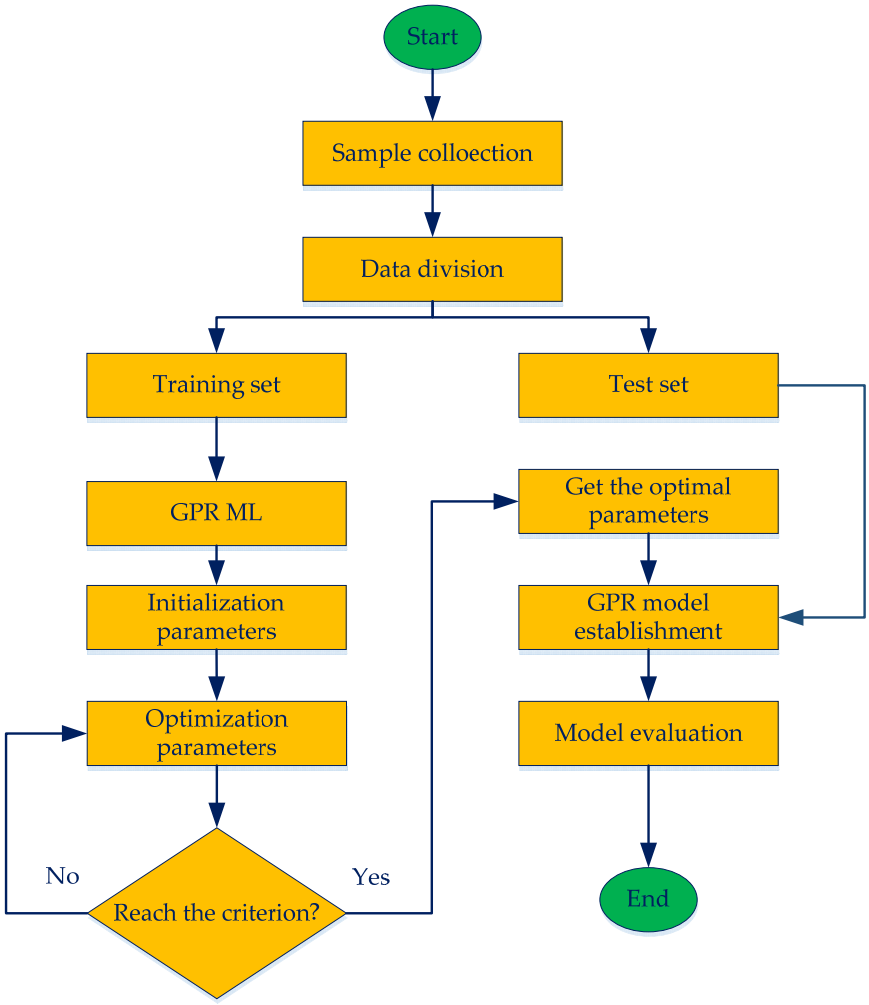

Figure 1. The flowchart associated with the prediction of ultimate bearing capacity using a data-driven approach.

5. Results and Discussion

The performance of the GPR model was evaluated using root-mean-square error (*RMSE*), coefficient of determination (R^2), the ratio of the root-mean-square error to the standard deviation of measured data (*RSR*), and Nash–Sutcliffe coefficient (*NSE*) and mean bias error (*MBE*). The results were compared with some popular classical methods suggested in the literature (i.e., Vesic [4]; Hansen [3]) for determining the UBC of shallow foundation on cohesionless soil. The GPR model in Section 3.3 was developed by learning from the 78 data, and the results of the training performance including R^2, *RSR*, *NSE*, and *MBE* are shown in Table 4. In comparison to the theoretical equations, the output of the GPR model on the testing phase has substantially higher values of coefficient of determination (R^2), Nash–Sutcliffe coefficient (*NSE*), and lower values of *MBE* and *RSR*. In addition, the equation proposed by Vesic [50] shows the best performance in comparison to the Hansen [3] theoretical formulas. Figure 2 shows the best-fit line of estimated versus measured UBC and the associated coefficient of determination (R^2). The outputs of the used theoretical formulas are more scattered than the GPR-based model, as shown in this Figure 2. From Table 4, it can be inferred that the R^2 and *NSE* are the highest (0.9404 and 0.8420), and the other criteria such as *RSR* and *MBE* are the least (0.8420 and −69.3268) for the GPR-based modeling in the testing phase. *MBE* (Vesic [4]: −105.2996 and Hansen [3]: −161.2911) has the largest negative score (see Table 5), indicating that it is the most conservative approach. It is clear that the GPR model is more accurate than analytical

formulas. The model performs better when R^2 and *NSE* values are greater than 0.85. Thus, it depicts the accuracy of the finalized model.

Table 4. Performance statistics of proposed model.

Performance Index	Training	Testing
R^2	0.9552	0.9404
RSR	0.3428	0.3975
NSE	0.8825	0.8420
MBE (kPa)	−10.9661	−69.3268

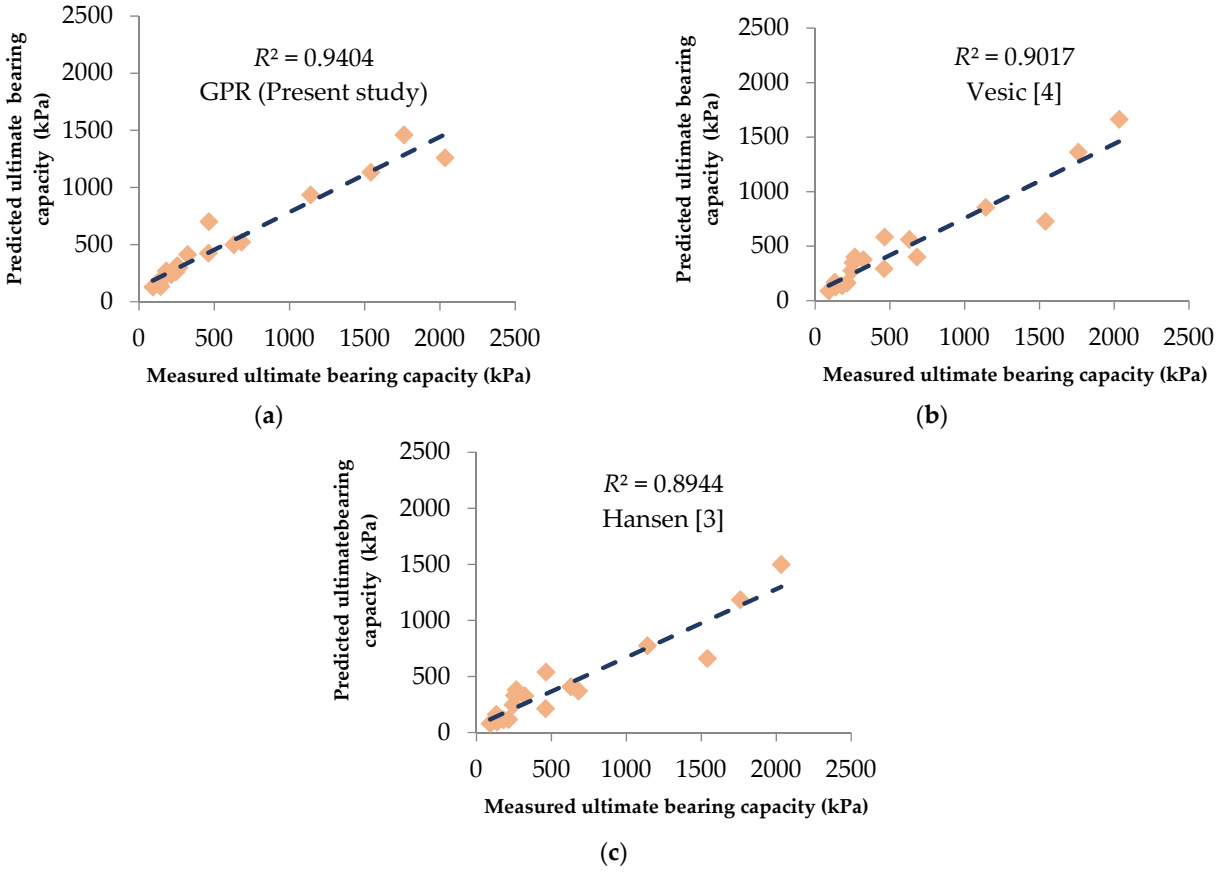

Figure 2. Scatter plot presenting the actual UBC values versus the predicted UBC on the testing dataset: (**a**) in GPR model (this study); (**b**) in Vesic [4]; (**c**) in Hansen [3].

Table 5. Performance statistics of bearing capacity theories.

Performance Index	Testing Set	
	Vesic [4]	Hansen [3]
R^2	0.9017	0.8944
RSR	0.4303	0.5227
NSE	0.8149	0.7268
MBE (kPa)	−105.2996	−161.2911

Figure 3 shows the comparison results of the training and testing sets to characterize the difference between the actual and predicted UBC of shallow foundations on cohesionless soil. Good agreements can be also observed between the comparison results, except for the few noise points, but these results are acceptable for the proposed GPR model to predict the UBC of shallow foundation on cohesionless soil.

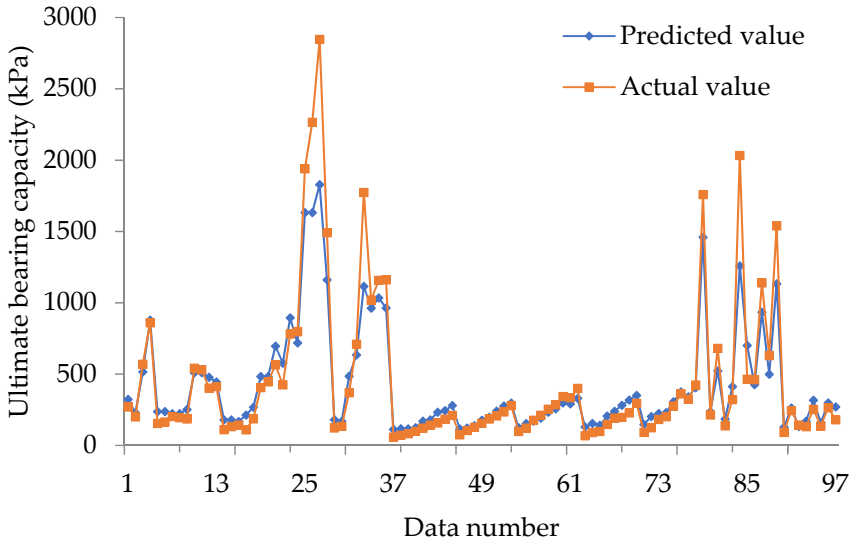

Figure 3. Actual versus predicted ultimate bearing capacity values.

The proposed model was developed and validated using data inside the data range (see Table 2), but it was not tested outside of this range; hence, it is assumed that the suggested model will be valid for data inside within the data range.

The GPR model's sensitivity results were evaluated using Yang and Zang's [51] technique to assess the influence of input parameters on q_u. This method has been utilized in a number of studies [14,52–54], and it is stated as follows:

$$r_{ij} = \frac{\sum_{m=1}^{n}(y_{im} \times y_{om})}{\sqrt{\sum_{m=1}^{n} y_{im}{}^2 \sum_{m=1}^{n} y_{om}{}^2}} \quad (11)$$

where n is the number of data values (this study used 78 data values); y_{im} and y_{om} are the input and output parameters. The r_{ij} value ranges from zero to one for each input parameter, and the highest r_{ij} values suggested the most efficient output parameter (which was q_u in this study). The r_{ij} values for all input parameters are presented in Figure 4. Figure 4, shows that the depth of foundation, D $(r_{ij} = 0.817)$ has the greatest effect on the UBC. The sensitivity results match well with the result of the investigations by Meyerhof [2] and Kohestani et al. [26].

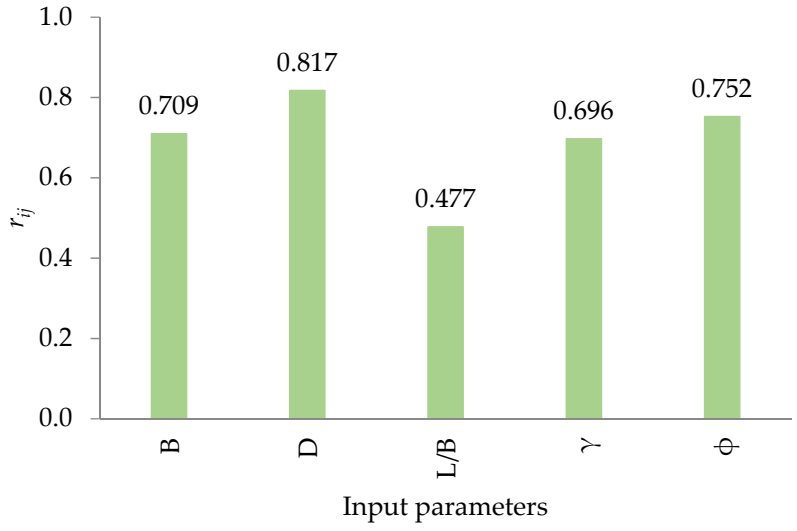

Figure 4. Sensitivity analysis of input parameters.

6. Conclusions

In this paper, using the GPR model, values of UBC of shallow foundations on cohesionless soil were estimated. Five input variables and one output variable were used for designing the prediction model. The modeling results reveal that the GPR model has an appropriate capability for accurate estimation of the UBC of cohesionless soil. The GPR-based model also provides improved performance compared with the conventional methods considered in this study. Results of sensitivity analysis conclude that the depth of foundation is the primary essential parameter when the GPR-based model is selected for estimation of the UBC of cohesionless soil for this dataset. For this dataset, the Pearson VII kernel function-based GPR model performs better and can be used in a variety of geotechnical engineering problems with inherent uncertainties and imperfections. Furthermore, the GPR technique has the advantage of being quickly updated as new data becomes available, avoiding the requirement for expertise and time to update the old design aid or equation and/or propose a new equation.

Author Contributions: Conceptualization, M.A., R.A.A.-M. and F.A.; methodology, F.A. and M.A.; software, F.A.; validation, F.A. and M.A.; formal analysis, M.A., R.A.A.-M. and F.A.; investigation, F.A., M.A. and M.A.; resources, M.A.; data curation, P.R.; writing—original draft preparation, F.A. and M.A.; writing—review and editing, P.R., P.W., M.S., P.K. and P.O.; supervision, P.W.; project administration, M.A., P.K. and P.W.; funding acquisition, P.K., P.W. and P.O. All authors have read and agreed to the published version of the manuscript.

Funding: This research received no external funding.

Institutional Review Board Statement: Not applicable.

Informed Consent Statement: Not applicable.

Data Availability Statement: The data used to support the findings of this study are included in the article.

Conflicts of Interest: The authors declare no conflict of interest.

Appendix A

Table A1. The data used for developing the GPR model.

S. No.	B (m)	D (m)	L/B	γ (kN/m^3)	ϕ (°)	q_u (kPa)
1	0.6	0.3	2	9.85	34.9	270
2	0.6	0	2	10.85	44.8	860
3	0.152	0.075	5.95	17.1	42.5	335.3
4	0.0585	0.058	5.95	16.8	41.5	184.9
5	0.5	0	1	11.7	37	111
6	0.5	0	2	11.7	37	143
7 *	0.5	0.3	1	10.2	37.7	681
8	0.152	0.15	1	16.1	37	182.4
9	0.0585	0.058	5.95	15.7	34	70.91
10 *	1	0	3	11.93	40	630
11	0.152	0.15	5.95	15.7	34	122.3
12	0.152	0.15	1	16.8	41.5	361.5
13 *	0.5	0.5	4	12	40	1140
14	0.5	0.029	4	11.7	37	109
15	0.5	0	1	10.2	37.7	154
16	0.094	0.094	6	17.1	42.5	279.6
17	0.094	0.047	1	16.1	37	98.8
18	0.5	0.5	2	12.41	44	2847
19	0.5	0	4	12.41	44	797
20	0.0585	0.029	5.95	16.1	37	82.5
21 *	0.152	0.075	1	16.1	37	135.2

Table A1. *Cont.*

S. No.	B (m)	D (m)	L/B	γ (kN/m^3)	ϕ (°)	q_u (kPa)
22	0.5	0.3	1	12.41	44	1940
23 *	0.152	0.15	1	16.5	39.5	264.5
24	0.5	0	2	10.2	37.7	195
25 *	0.6	0.3	2	10.85	44.8	1760
26	0.991	0.711	1	15.8	32	1773.7
27	0.5	0.3	1	11.7	37	446
28	0.5	0	1	10.2	37.7	165
29	0.5	0	1	11.77	37	123
30	0.5	0.49	4	12.27	42	1492
31	0.152	0.15	5.95	16.8	41.5	342.5
32	0.094	0.094	6	16.5	39.5	185.6
33	0.5	0	1	11.7	37	132
34	0.5	0	2	10.2	37.7	203
35 *	0.5	0.3	4	11.7	37	322
36	0.094	0.094	1	15.7	34	90.5
37	0.094	0.047	6	16.8	41.5	206.8
38	0.094	0.047	6	16.1	37	104.8
39	2.489	0.762	1	15.8	32	1158
40	0.094	0.094	1	16.5	39.5	191.6
41	0.152	0.075	5.95	15.7	34	98.2
42	0.094	0.047	1	16.5	39.5	147.8
43	0.5	0.127	4	11.7	37	187
44 *	0.5	0.5	4	12.41	44	2033
45 *	0.094	0.094	1	16.8	41.5	253.6
46	0.5	0.3	3	10.2	37.7	402
47	3.004	0.762	1	15.8	32	1019.4
48	0.152	0.075	1	16.8	41.5	276.3
49	0.094	0.047	6	17.1	42.5	235.6
50	0.152	0.15	5.95	16.1	37	176.4
51	0.6	0.3	2	10.2	37.7	570
52	0.5	0.3	1	11.77	37	370
53	0.5	0.3	2	10.2	37.7	530
54	0.094	0.047	1	16.8	41.5	196.8
55 *	0.094	0.094	6	16.8	41.5	244.6
56	0.094	0.094	1	17.1	42.5	295.6
57	0.152	0.15	5.95	16.5	39.5	254.5
58	0.52	0	3.85	10.2	37.7	186
59	0.152	0.15	5.95	17.1	42.5	400.6
60	1	0.2	3	11.97	39	710
61	0.0585	0.029	5.95	15.7	34	58.5
62 *	0.5	0.013	1	11.7	37	137
63	0.5	0.3	1	12.41	44	2266
64	0.0585	0.029	5.95	16.5	39.5	121.5
65	0.5	0.5	4	11.7	37	425
66	0.094	0.094	6	16.1	37	127.5
67 *	0.0585	0.029	5.95	17.1	42.5	180.5
68	0.152	0.075	1	15.7	34	91.2
69 *	0.152	0.075	5.95	16.1	37	143.3
70	0.094	0.047	1	15.7	34	67.7
71	0.152	0.075	1	17.1	42.5	325.3
72	0.094	0.047	1	17.1	42.5	228.8
73	0.5	0.3	2	10.2	37.7	542
74	0.094	0.047	6	15.7	34	74.7
75	0.094	0.047	6	16.5	39.5	155.8
76 *	1.492	0.762	1	15.8	32	1540
77	0.5	0	1	12.41	44	782
78	0.6	0	2	10.2	37.7	200
79	0.152	0.075	5.95	16.5	39.5	211.2
80	0.5	0.5	2	11.7	37	565

Table A1. *Cont.*

S. No.	B (m)	D (m)	L/B	γ (kN/m^3)	ϕ (°)	q_u (kPa)
81	0.152	0.15	1	17.1	42.5	423.6
82 *	0.5	0.5	2	11.77	37	464
83	0.152	0.075	5.95	16.8	41.5	285.3
84 *	0.094	0.094	1	16.1	37	131.5
85	0.0585	0.058	5.95	17.1	42.5	211
86	0.152	0.075	1	16.5	39.5	201.2
87	0.0585	0.058	5.95	16.5	39.5	142.9
88	0.0585	0.058	5.95	16.1	37	98.93
89	0.152	0.15	1	15.7	34	124.4
90 *	0.5	0	3	10.2	37.7	214
91	0.0585	0.029	5.95	16.8	41.5	157.5
92 *	0.094	0.094	6	15.7	34	91.5
93 *	0.5	0	4	12	40	461
94	0.52	0.3	3.85	10.2	37.7	413
95	3.016	0.889	1	15.8	32	1161.2
96	0.5	0	2	11.77	37	134
97	0.5	0.3	1	11.7	37	406

Note: * presents the test set.

References

1. Terzaghi, K. *Theoretical Soil Mechanics*; John Wiley and Sons: New York, NY, USA, 1943.
2. Meyerhof, G.G. Some recent research on the bearing capacity of foundations. *Can. Geotech. J.* **1963**, *1*, 16–26. [CrossRef]
3. Hansen, J.B. *A Revised and Extended Formula for Bearing Capacity*; Danish Geotechnical Institute: Lyngby, Denmark, 1970.
4. Vesic, A. Bearing Capacity of Shallow Foundations. In *Foundation Engineering Handbook*; Winterkorn, F.S., Fand, H.Y., Eds.; Van Nostrand Reinhold: New York, NY, USA, 1975.
5. Das, B. *Principles of Foundation Engineering*; Brooks/Cole-Thomson Learning, Inc.: Boston, MA, USA, 2004; p. 489.
6. Conte, E.; Pugliese, L.; Troncone, A.; Vena, M. A simple approach for evaluating the bearing capacity of piles subjected to inclined loads. *Int. J. Geomech.* **2021**, *21*, 04021224. [CrossRef]
7. Achmus, M.; Thieken, K. On the behavior of piles in non-cohesive soil under combined horizontal and vertical loading. *Acta Geotechnica* **2010**, *5*, 199–210. [CrossRef]
8. De Beer, E. The scale effect on the phenomenon of progressive rupture in cohesionless soils. In Proceedings of the 6th ICSMFE, Montreal, QC, Canada, 8–15 September 1965; pp. 13–17.
9. Yamaguchi, H. On the scale effect of footings in dense sand. In Proceedings of the 9th ICSMFE, Tokyo, Japan, 10–15 July 1977; pp. 795–798.
10. Tatsuoka, T. Progressive failure and particle size effect in bearing capacity of footing on sand. *ASCE Geotech. Spec. Publ.* **1991**, *27*, 788–802.
11. Padmini, D.; Ilamparuthi, K.; Sudheer, K. Ultimate bearing capacity prediction of shallow foundations on cohesionless soils using neurofuzzy models. *Comput. Geotech.* **2008**, *35*, 33–46. [CrossRef]
12. Ahmad, M.; Tang, X.-W.; Qiu, J.-N.; Ahmad, F. Evaluation of liquefaction-induced lateral displacement using Bayesian belief networks. *Front. Struct. Civ. Eng.* **2021**, *15*, 80–98. [CrossRef]
13. Ali Khan, M.; Zafar, A.; Akbar, A.; Javed, M.F.; Mosavi, A. Application of Gene Expression Programming (GEP) for the Prediction of Compressive Strength of Geopolymer Concrete. *Materials* **2021**, *14*, 1106. [CrossRef] [PubMed]
14. Ahmad, M.; Hu, J.-L.; Ahmad, F.; Tang, X.-W.; Amjad, M.; Iqbal, M.J.; Asim, M.; Farooq, A. Supervised Learning Methods for Modeling Concrete Compressive Strength Prediction at High Temperature. *Materials* **2021**, *14*, 1983. [CrossRef] [PubMed]
15. Ahmad, M.; Tang, X.-W.; Qiu, J.-N.; Gu, W.-J.; Ahmad, F. A hybrid approach for evaluating CPT-based seismic soil liquefaction potential using Bayesian belief networks. *J. Cent. South Univ.* **2020**, *27*, 500–516.
16. Pirhadi, N.; Tang, X.; Yang, Q.; Kang, F. A new equation to evaluate liquefaction triggering using the response surface method and parametric sensitivity analysis. *Sustainability* **2019**, *11*, 112. [CrossRef]
17. Ahmad, M.; Tang, X.; Ahmad, F. Evaluation of Liquefaction-Induced Settlement Using Random Forest and REP Tree Models: Taking Pohang Earthquake as a Case of Illustration. In *Natural Hazards-Impacts, Adjustments & Resilience*; IntechOpen: London, UK, 2020.
18. Ahmad, M.; Al-Shayea, N.A.; Tang, X.-W.; Jamal, A.; Al-Ahmadi, H.M.; Ahmad, F. Predicting the Pillar Stability of Underground Mines with Random Trees and C4. 5 Decision Trees. *Appl. Sci.* **2020**, *10*, 6486. [CrossRef]
19. Ahmad, M.; Tang, X.-W.; Qiu, J.-N.; Ahmad, F.; Gu, W.-J. A step forward towards a comprehensive framework for assessing liquefaction land damage vulnerability: Exploration from historical data. *Front. Struct. Civ. Eng.* **2020**, *14*, 1476–1491. [CrossRef]

20. Zhou, J.; Li, E.; Wang, M.; Chen, X.; Shi, X.; Jiang, L. Feasibility of stochastic gradient boosting approach for evaluating seismic liquefaction potential based on SPT and CPT case histories. *J. Perform. Constr. Facil.* **2019**, *33*, 04019024. [CrossRef]
21. Hamdia, K.M.; Arafa, M.; Alqedra, M. Structural damage assessment criteria for reinforced concrete buildings by using a Fuzzy Analytic Hierarchy process. *Undergr. Space* **2018**, *3*, 243–249. [CrossRef]
22. Kalinli, A.; Acar, M.C.; Gündüz, Z. New approaches to determine the ultimate bearing capacity of shallow foundations based on artificial neural networks and ant colony optimization. *Eng. Geol.* **2011**, *117*, 29–38. [CrossRef]
23. Samui, P. Application of statistical learning algorithms to ultimate bearing capacity of shallow foundation on cohesionless soil. *Int. J. Numer. Anal. Methods Geomech.* **2012**, *36*, 100–110. [CrossRef]
24. Shahnazari, H.; Tutunchian, M.A. Prediction of ultimate bearing capacity of shallow foundations on cohesionless soils: An evolutionary approach. *KSCE J. Civ. Eng.* **2012**, *16*, 950–957. [CrossRef]
25. Tsai, H.-C.; Tyan, Y.-Y.; Wu, Y.-W.; Lin, Y.-H. Determining ultimate bearing capacity of shallow foundations using a genetic programming system. *Neural Comput. Appl.* **2013**, *23*, 2073–2084. [CrossRef]
26. Kohestani, V.R.; Vosoghi, M.; Hassanlourad, M.; Fallahnia, M. Bearing capacity of shallow foundations on cohesionless soils: A random forest based approach. *Civ. Eng. Infrastruct. J.* **2017**, *50*, 35–49.
27. Hewing, L.; Kabzan, J.; Zeilinger, M.N. Cautious model predictive control using gaussian process regression. *IEEE Trans. Control. Syst. Technol.* **2019**, *28*, 2736–2743. [CrossRef]
28. Sun, A.Y.; Wang, D.; Xu, X. Monthly streamflow forecasting using Gaussian process regression. *J. Hydrol.* **2014**, *511*, 72–81. [CrossRef]
29. Roushangar, K.; Shahnazi, S. Prediction of sediment transport rates in gravel-bed rivers using Gaussian process regression. *J. Hydroinform.* **2020**, *22*, 249–262. [CrossRef]
30. Prandtl, L. On the penetrating strengths (hardness) of plastic construction materials and the strength of cutting edges. *ZAMM J. Appl. Math. Mech.* **1921**, *1*, 15–20. [CrossRef]
31. Reissner, H. Zum erddruckproblem. In Proceedings of the 1st International Congress for Applied Mechanics, Delft, The Netherlands, 22–26 April 1924; pp. 295–311.
32. Taylor, D. *Fundamentals of Soil Mechanics*; John Wiley & Sons: New York, NY, USA; Chapman & Hall: London, UK, 1948.
33. Vesić, A.S. Analysis of ultimate loads of shallow foundations. *J. Soil Mech. Found. Div.* **1973**, *99*, 45–73. [CrossRef]
34. Cerato, A. Scale Effects of Foundation Bearing Capacity on Granular Material. Ph.D. Dissertation, Lafayette College, University of Massachusetts Amherst, Amherst, MA, USA, 2005.
35. Ahmad, M.; Tang, X.-W.; Qiu, J.-N.; Ahmad, F. Evaluating Seismic Soil Liquefaction Potential Using Bayesian Belief Network and C4. 5 Decision Tree Approaches. *Appl. Sci.* **2019**, *9*, 4226. [CrossRef]
36. Javadi, A.A.; Rezania, M.; Nezhad, M.M. Evaluation of liquefaction induced lateral displacements using genetic programming. *Comput. Geotech.* **2006**, *33*, 222–233. [CrossRef]
37. Van Vuren, T. *Modeling of Transport Demand–Analyzing, Calculating, and Forecasting Transport Demand*; Elsevier: Amsterdam, The Netherlands, 2018; p. 472.
38. Song, Y.; Gong, J.; Gao, S.; Wang, D.; Cui, T.; Li, Y.; Wei, B. Susceptibility assessment of earthquake-induced landslides using Bayesian network: A case study in Beichuan, China. *Comput. Geosci.* **2012**, *42*, 189–199. [CrossRef]
39. Zhao, K.; Popescu, S.; Meng, X.; Pang, Y.; Agca, M. Characterizing forest canopy structure with lidar composite metrics and machine learning. *Remote Sens. Environ.* **2011**, *115*, 1978–1996. [CrossRef]
40. Pasolli, L.; Melgani, F.; Blanzieri, E. Gaussian process regression for estimating chlorophyll concentration in subsurface waters from remote sensing data. *IEEE Geosci. Remote Sens. Lett.* **2010**, *7*, 464–468. [CrossRef]
41. Rasmussen, C.; Williams, C. *Gaussian Processes for Machine Learning*; The MIT Press: Cambridge, MA, USA, 2006; Volume 35, pp. 715–719.
42. Bazi, Y.; Alajlan, N.; Melgani, F.; AlHichri, H.; Yager, R.R. Robust estimation of water chlorophyll concentrations with gaussian process regression and IOWA aggregation operators. *IEEE J. Sel. Top. Appl. Earth Obs. Remote Sens.* **2014**, *7*, 3019–3028. [CrossRef]
43. Kumar, M.; Elbeltagi, A.; Srivastava, A.; Kumari, A.; Ali, R.; Pande, C.; Bajirao, T.S.; Islam, A.R.M.T.; Kushwaha, D.P. Prediction of Daily Streamflow Using Various Kernel Function Based Regression: A Case Study in India. Preprint. 2021. Available online: https://assets.researchsquare.com/files/rs-784271/v1_covered.pdf?c=1631876022 (accessed on 24 September 2021).
44. Gandomi, A.H.; Babanajad, S.K.; Alavi, A.H.; Farnam, Y. Novel approach to strength modeling of concrete under triaxial compression. *J. Mater. Civ. Eng.* **2012**, *24*, 1132–1143. [CrossRef]
45. Nush, J.; Sutcliffe, J.V. River flow forecasting through conceptual models part I—A discussion of principles. *J. Hydrol.* **1970**, *10*, 282–290. [CrossRef]
46. Moriasi, D.N.; Arnold, J.G.; van Liew, M.W.; Bingner, R.L.; Harmel, R.D.; Veith, T.L. Model evaluation guidelines for systematic quantification of accuracy in watershed simulations. *Trans. ASABE* **2007**, *50*, 885–900. [CrossRef]
47. Khosravi, K.; Mao, L.; Kisi, O.; Yaseen, Z.M.; Shahid, S. Quantifying hourly suspended sediment load using data mining models: Case study of a glacierized Andean catchment in Chile. *J. Hydrol.* **2018**, *567*, 165–179. [CrossRef]
48. Witten, I.H.; Frank, E.; Hall, M. *Data Mining: Practical Machine Learning Tools and Techniques*; Morgen Kaufmann: San Francisco, CA, USA, 2005.
49. Üstün, B.; Melssen, W.J.; Buydens, L.M. Facilitating the application of support vector regression by using a universal Pearson VII function based kernel. *Chemom. Intellig. Lab. Syst.* **2006**, *81*, 29–40. [CrossRef]

50. Vesić, A.S. Closure to "Analysis of Ultimate Loads of Shallow Foundations". *J. Geotech. Eng. Div.* **1974**, *100*, 949–952. [CrossRef]
51. Yang, Y.; Zhang, Q. A hierarchical analysis for rock engineering using artificial neural networks. *Rock Mech. Rock Eng.* **1997**, *30*, 207–222. [CrossRef]
52. Faradonbeh, R.S.; Armaghani, D.J.; Abd Majid, M.; Tahir, M.M.; Murlidhar, B.R.; Monjezi, M.; Wong, H. Prediction of ground vibration due to quarry blasting based on gene expression programming: A new model for peak particle velocity prediction. *Int. J. Environ. Sci. Technol.* **2016**, *13*, 1453–1464. [CrossRef]
53. Chen, W.; Hasanipanah, M.; Rad, H.N.; Armaghani, D.J.; Tahir, M. A new design of evolutionary hybrid optimization of SVR model in predicting the blast-induced ground vibration. *Eng. Comput.* **2021**, *37*, 1455–1471. [CrossRef]
54. Rad, H.N.; Bakhshayeshi, I.; Jusoh, W.A.W.; Tahir, M.; Foong, L.K. Prediction of flyrock in mine blasting: A new computational intelligence approach. *Nat. Resour. Res.* **2020**, *29*, 609–623.